Repeatability indicators in time lapse seismology and their application to the Sleipner CO_2 storage project

Brian Russell[1]

GeoSoftware, Calgary, Alberta, brian.russell@geosoftware.com

ABSTRACT

I compare three repeatability measures using the time lapse data from Sleipner CO_2 storage project in offshore Norway. The three repeatability are *NRMS*, predictability, and cross-correlation coefficient. I first review the work of Kragh and Christie (2002) who used NRMS and predictability and created a random noise model to explain their relationship. Using the Sleipner dataset, I show an excellent fit to their theory. I then review the work of Coléou et al. (2013), who used NRMS and cross-correlation measures and introduced two new attributes: quality Indicator (*Q*) and anomaly indicator (*A*). After discussing the relationship between predictability and cross-correlation I apply the *Q* and *A* attributes to the Sleipner dataset, showing how well the CO_2 plume can be identified.

INTRODUCTION

The Sleipner storage CO_2 project is roughly halfway between Scotland and Norway, in the Norwegian sector of the North Sea, as shown in the inset in Figure 1, from Ghaderi and Landrø (2009).

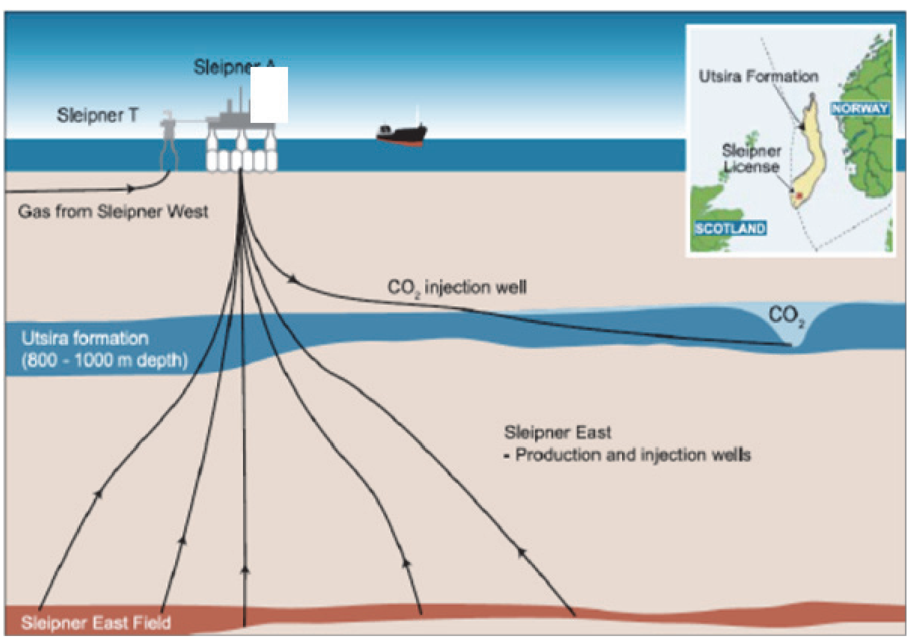

Figure 1. Geology of the Sleipner CO_2 storage project (Ghaderi and Landrø, 2009).

As shown in Figure 1, CO_2 is separated from the produced gas in the Sleipner West Gas Field and injected into the Utsira saline formation. The Utsira formation is 800-1000 m deep, highly porous (36-40%) and permeable (1-8 D).

Approximately 1 million tons of CO_2 per year has been injected into Sleipner since 1996. Seismic monitoring started with a base survey in 1984. Monitor surveys were done in 1999, 2001, 2004, 2006, 2008, and 2010 (Figure 2). This 4D dataset was released to the public by Equinor and is freely downloadable. Note also in Figure 2 that by 2010, 12 Mt of CO_2 had been injected into the reservoir.

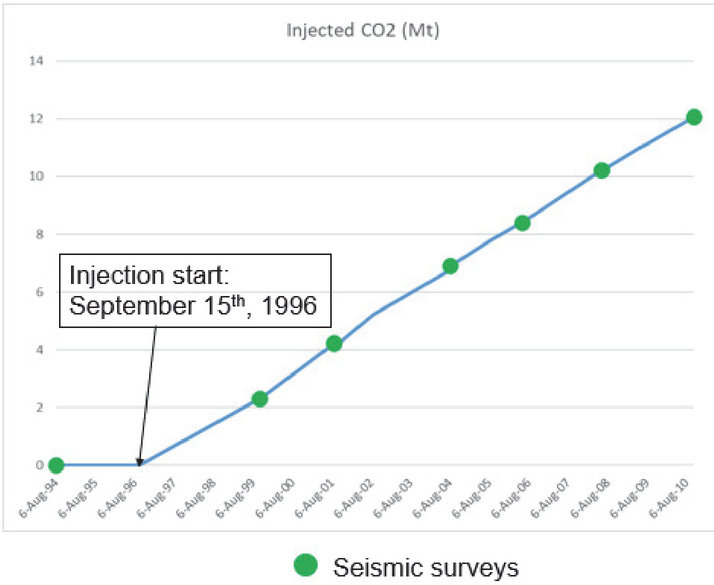

Figure 2. Time lapse surveys over Sleipner versus injected CO_2.

The Sleipner seismic dataset consists of 28 volumes, the full, near, mid, and far stacks for each of the seven vintages of data: 1994,1999, 2001, 2004, 2006, 2008 and 2010. Figure 3 shows the base map of the 3D survey, which contains 249 in-lines, from 1720 on the west to 1998 on the east, and 468 crosslines, from 898 on the south to 1458 on the north.

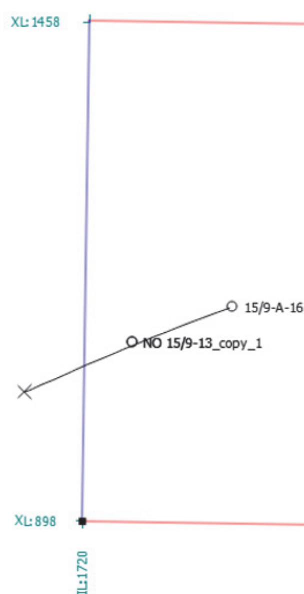

Figure 3. The seismic base map with available wells shown.

Two wells were available: the 15/9-A-16 injection well and the NO 15/9-13 well, which was outside the injection zone, also shown in Figure 3. The well log curves from the NO 15/9-13 well, which is outside the injection zone, are shown in Figure 4. Sonic (P-wave), density and Gamma Ray are measured curves, but the dipole sonic (S-wave) has been estimated using the Greenberg-Castagna relationship. Note the top and Base of Utsira picks, which show the extent of the injection zone.

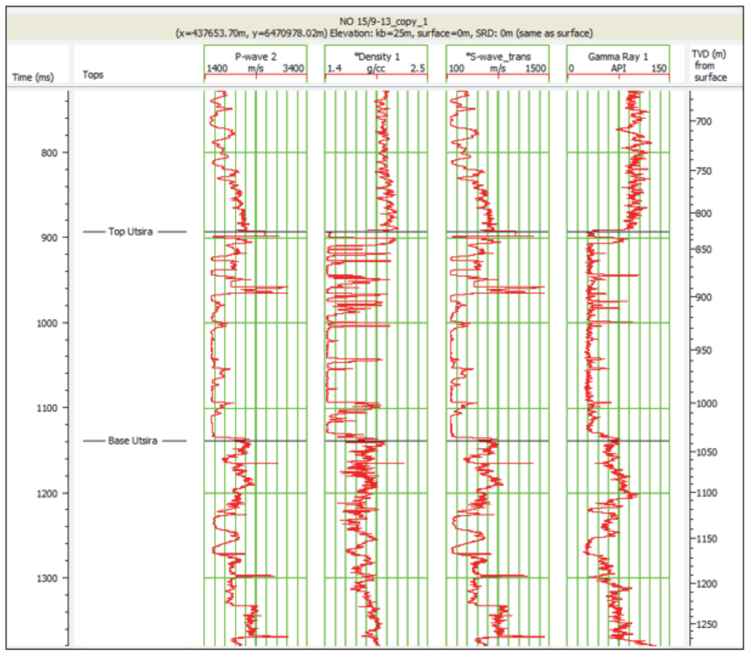

Figure 4. The well log curves from the NO 15/9-13 well, showing the top and base of the Utsira sand injection zone.

Figure 5 A display of the full stacks of inline 1871 (over the injection zone) showing the base and monitor sections from 1994 to 2010. Notice the clear expansion of the injected CO_2 plume.

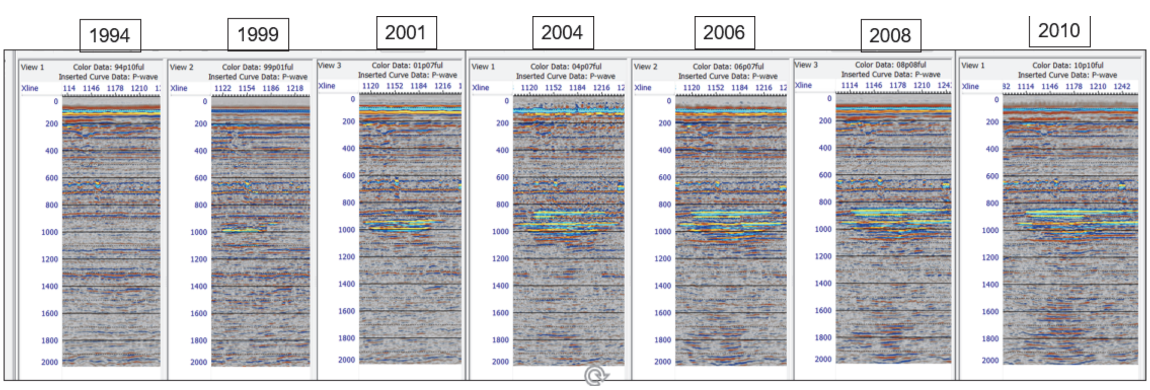

Figure 5. The full stacks from line 1871 (which is over the injection zone) from 1994 to 2010.

Figure 6 next shows the difference sections for inline 1871 between the 1994 base survey and the six monitor sections clearly show the expansion of the CO2 plume.

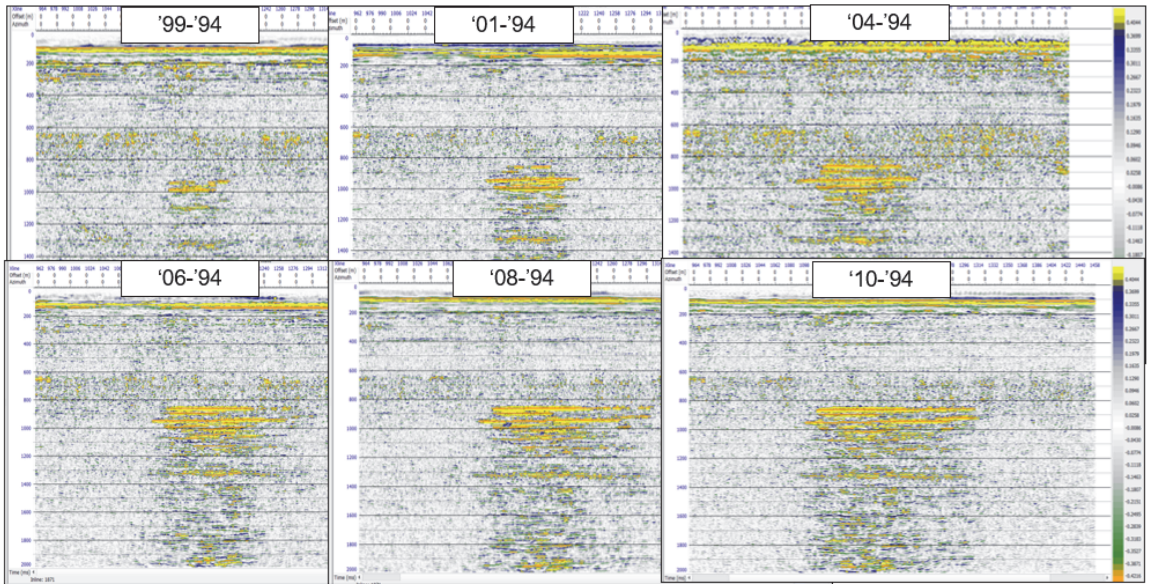

Figure 6. The difference sections for inline 1871 between the 1994 base survey and the six monitor sections.

Having looked at the geology of the Sleipner project and the input seismic data, I will next describe the theory behind time lapse repeatability indicators before applying these indicators to the Sleipner dataset.

THEORY

The three repeatability measures I will use in this study are the normalized root-mean-square (*NRMS*) approach, predictability (*PRED*), and cross-correlation coefficient (ρ). Let's first review the work of Kragh and Christie (2002) who used *NRMS* and *PRED* as their two indicators. *NRMS* between the base (b) and monitor (m) is defined as

$$NRMS = \frac{200\left[RMS(m-b)\right]}{RMS(m)+RMS(b)}, \tag{1}$$

where $RMS(x_t) = \sqrt{\dfrac{1}{N+1}\displaystyle\sum_{t=t_0}^{t_N} x_t^2}$ is the RMS estimate over trace samples x_t using a time window from $t = t_0$ to $t = t_N$. Note that the limits of the *NRMS* are from 0 to 200. The predictability, or *PRED*, is defined as

$$PRED = \frac{\displaystyle\sum_{\tau=-\max lag}^{\max lag} \phi_{bm}{}^2(\tau)}{\displaystyle\sum_{\tau=-\max lag}^{\max lag} \phi_{bb}(\tau) \sum_{\tau=-\max lag}^{\max lag} \phi_{mm}(\tau)}, \tag{2}$$

where $\phi_{bm}(\tau)$ is the cross-correlation between the base and monitor traces from lags between -and +max lag, $\phi_{bb}(\tau)$ is the autocorrelation of the base trace, and $\phi_{mm}(\tau)$ is the autocorrelation of the monitor trace between the same lags. The limits of the predictability are form 0 to 100%.

It is important to use the same time window over each seismic trace that was used in the *NRMS* calculation as input to the correlation process.

Kragh and Christie (2002) then show that the relationship between *NRMS* and *PRED* can be computed theoretically when adding random, or white, noise to a reference trace, and comparing the noisy trace to the original reference trace. The formulae for the two repeatability measures are given as

$$NRMS = \frac{141}{\sqrt{1+\frac{1}{\lambda^2}}}, \tag{3}$$

and

$$PRED = \frac{100}{\left(1+\lambda^2\right)^2}, \tag{4}$$

where λ is the ratio of the white noise amplitude to the seismic amplitude. Notice that the highest value of NRMS is now 141 rather than 200, which comes from the theoretical definition of signal-to-noise ratio. To visualize these relationships, Figure 7 shows plots of *NRMS* versus λ and *PRED* versus λ for values of λ from 0.01 to 10.

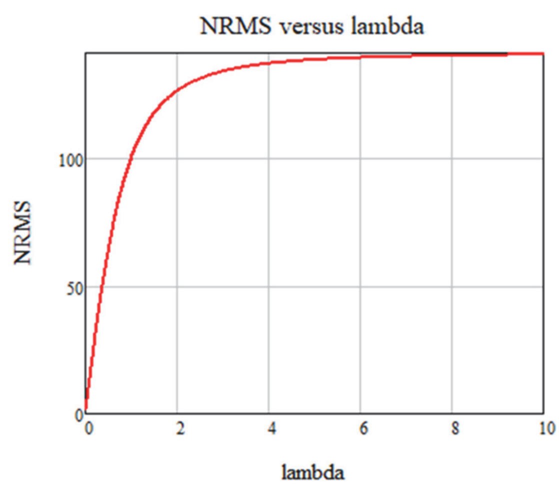

(a)

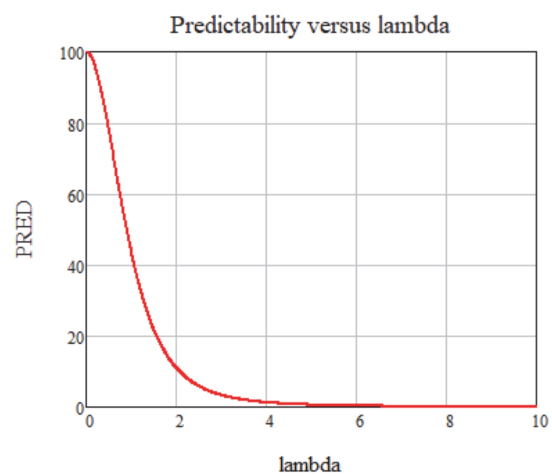

(b)

Figure 7. Plots of (a) NRMS vs λ, and (b) PRED vs λ, as given in equations 3 and 4.

Figure 8 then next shows the cross-plot of *PRED* versus *NRMS* over the same range of λ values as in Figure 7. Notice that this plot has a bell, or Gaussian, shape.

In the next section we will find that the real data cross-plots derived from the Sleipner dataset conform very well to this theoretical shape.

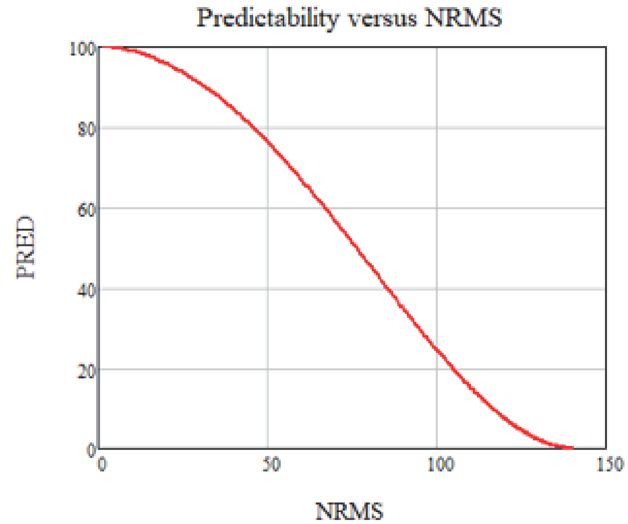

Figure 8. Plots of PRED versus NRMS from the relationships in equation 3 and 4.

The third repeatability indicator, correlation coefficient, or ρ, is the ratio of the maximum cross-correlation value at lag $\tau_{\max}$ divided by the product of the square roots of the autocorrelations, or

$$\rho = \frac{\phi_{bm}(\tau_{\max})}{\sqrt{\phi_{bb}(\tau_{\max})}\sqrt{\phi_{mm}(\tau_{\max})}}. \tag{5}$$

Notice that the correlation coefficient finds a single correlation coefficient, whereas the predictability computes an *RMS* average of a series of lags. The advantage of using cross-correlation is that the time shift $\tau_{\max}$ between the base and monitor surveys can be used to align the two surveys. The advantage of the predictability measurement is that it gives a smoothed correlation result.

To quantify the amount of smoothing that occurs when using predictability as compared to correlation coefficient with, Kragh and Christie (2002) assume that the effect the number of lags used in the computation of predictability can be simulated by adding a damping factor to the equation 4, or

$$PRED = \frac{100}{\left(1 + d\lambda^2\right)^2}, \tag{6}$$

where d is the damping factor.

Figure 9 shows the cross-plot between NRMS and the damped predictability of equation (6), where we display curves using three different values of the damping factor d: 0.5, 0.75 and 1.0. In their paper, Kragh and Christie (2002) use a damping factor of 0.75. Notice that at a damping factor of 0.5 the Gaussian shape of the curve starts to look more like a parabola.

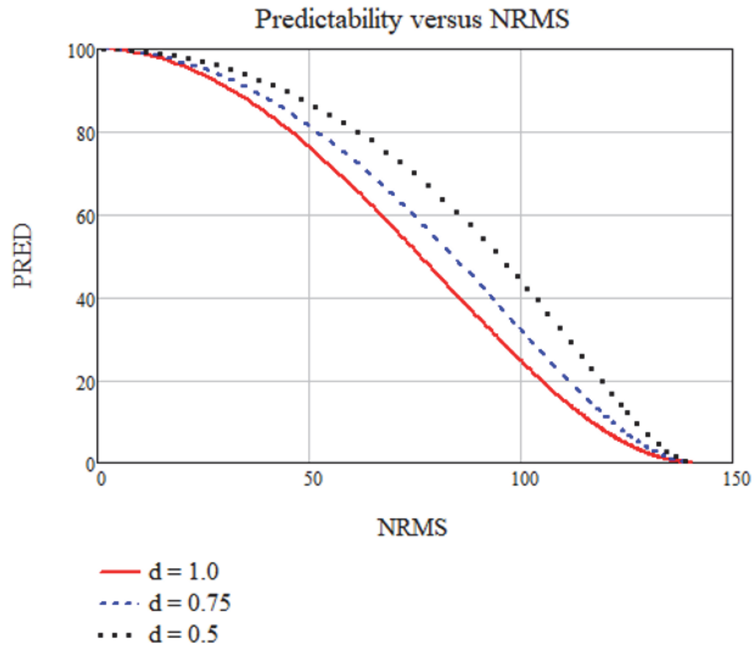

Figure 9. Plots of damped PRED from equation 6 versus NRMS, where three different values of the damping factor d have been used.

Coléou et al. (2013) extended the work of Kragh and Christie (2002) by considering the statistics behind ρ and *NRMS* and using these two measures in their cross-plot. Figure 10 shows a set of points from a 4D survey with two curves superimposed. Notice that they have normalized the Kragh and Christie (2002) limits by dividing by 100.

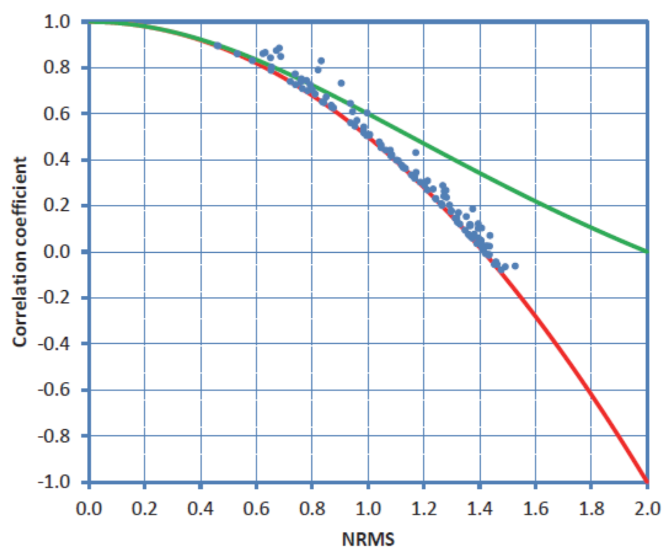

Figure 10. Cross-plot of correlation coefficient ρ versus NRMS where the blue points are from a real data survey and the red and green lines are defined in equations 7 and 8, (Coléou et al., 2013).

In Figure 10, the blue data points come from a seismic survey, and the red and green curves represent bounds on the data that will be defined next.

The red curve is the lower bound when the two datasets have the same variance, and can be written as

$$\rho = 1 - \frac{NRMS^2}{2}. \tag{7}$$

The green curve is the lower bound when we add random noise to a seismic trace and compare the traces, and can be written as

$$\rho = \frac{4 - NRMS^2}{4 + NRMS^2}. \tag{8}$$

Notice that the green curve is almost identical to Kragh and Christie's equation with a damping factor of 0.5, as shown in Figure 9.

Coléou et al. (2013) also introduced two new repeatability indicators. The first is called the quality indicator, Q, which they define mathematically as

$$Q = \frac{\rho - NRMS^2/2}{4} + \frac{3}{4}, \tag{9}$$

where $NRMS = \dfrac{2\sigma(b-m)}{\sigma(b)+\sigma(m)}$, $\rho = \dfrac{Cov[b,m]}{\sigma(b)\sigma(m)}$, $\sigma =$ std. deviation, $Cov =$ covariance, and b and m are the base and monitor surveys, respectively. I have arranged equation 9 slightly differently than Coléou et al. (2013) to make it more interpretable. Notice that the equation consists of the difference between ρ and $NRMS^2/2$ divided by 4 with an added term of 3/4. Figure 11(a) shows a plot of ρ versus $NRMS^2/2$ and Figure 11(b) shows a plot of ρ versus $NRMS$, where both plots show lines of constant Q.

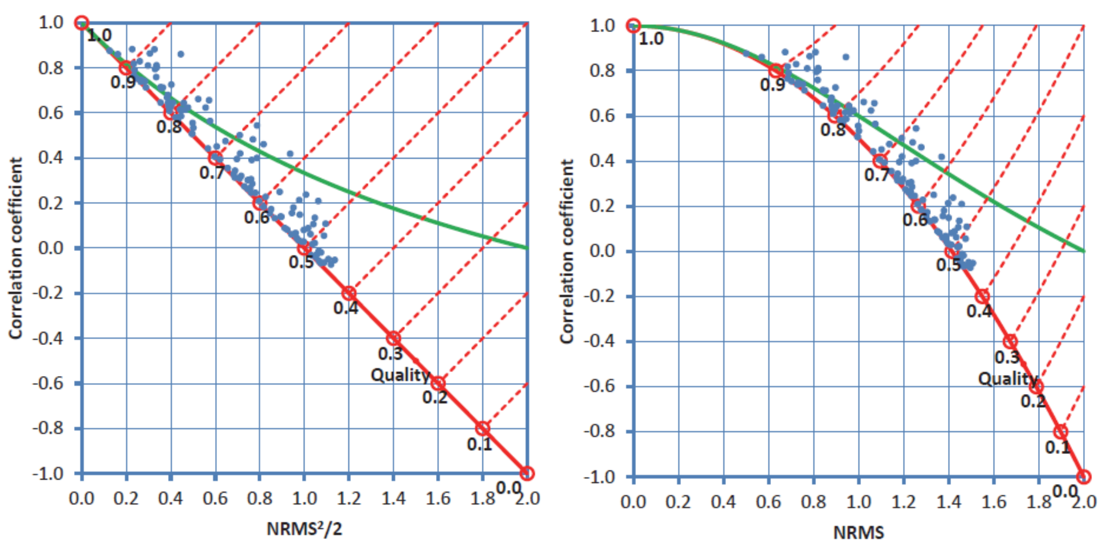

(a) (b)

Figure 11. Plot of (a) ρ vs $NRMS^2/2$, and (b) ρ vs NRMS, showing lines of Q constant (Coléou et al., 2013).

The easiest way to understand the motivation for the Quality indicator Q is to look at Figure 11(a) first, since the relationship is best understood as a function of $NRMS^2/2$, as shown in equation 9, which makes the relationship linear. First, consider the solid red line, which is the lower bound that corresponds to two traces with the same variance. Table 1 shows the computation of Q on this line using equation 9, and shows that Q goes from 1.0, where ρ is maximum and $NRMS^2/2$ is minimum, to 0.0, where ρ is minimum and $NRMS^2/2$ is maximum.

Rho	NRMS^2/2	(Rho-NRMS^2/2)/4	Q
1.0	0.0	0.25	1.0
0.8	0.2	0.15	0.9
0.6	0.4	0.05	0.8
0.4	0.6	-0.05	0.7
0.2	0.8	-0.15	0.6
0.0	1.0	-0.25	0.5
-0.2	1.2	-0.35	0.4
-0.4	1.4	-0.45	0.3
-0.6	1.6	-0.55	0.2
-0.8	1.8	-0.65	0.1
-1.0	2.0	-0.75	0.0

Table 1. Computation of Q on the lower bound line.

Now, let's look at the dashed red lines on figure 10(a), which represent lines of constant Q. By shifting $NRMS^2/2$ by 0.4 we get the end of the dashed red line at $\rho = 1.0$. Table 2 shows the computations that prove this is correct. Notice that this table stops at $\rho = -0.6$, which corresponds to the end of the dashed red line of with constant Q equal to 0.1.

Rho	NRMS^2/2 + 0.4	(Rho-NRMS^2/2)/4	Q
1.0	0.4	0.15	0.9
0.8	0.6	0.05	0.8
0.6	0.8	-0.05	0.7
0.4	1.0	-0.15	0.6
0.2	1.2	-0.25	0.5
0.0	1.4	-0.35	0.4
-0.2	1.6	-0.45	0.3
-0.4	1.8	-0.55	0.2
-0.6	2.0	-0.65	0.1

Table 2. Computation of Q with $NRMS^2/2$ shifted by 0.4.

Going back to Figure 11(b), where $NRMS$ is plotted on the X-axis, we see that the lines of constant Q still radiate outwards from the lower bound, but they are now nonlinear. As mentioned earlier, we gain more physical insight into this line by looking at Figure 11(a).

The second indicator defined by Coléou et al. (2013) is called the anomaly indicator A, which is defined mathematically as

$$A = \frac{\rho + NMRS^2 / 2}{2} - \frac{1}{2}, \tag{10}$$

Again, I have arranged equation 10 slightly differently than Coléou et al. (2013) did to make it more interpretable. This equation differs from equation 9 in that it consists of the sum of ρ and $NRMS^2/2$, rather than the difference, which is divided by 2 and has a subtracted term of 1/2. Figure 12(a) shows a plot of ρ versus $NRMS^2/2$ and Figure 12(b) shows a plot of ρ versus $NRMS$, where both plots now show lines of constant A.

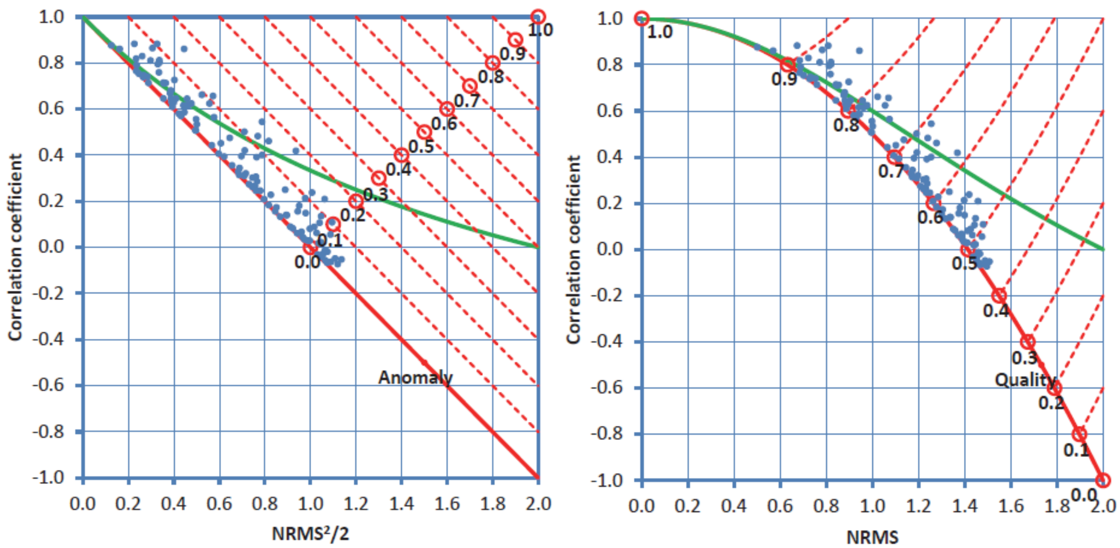

(a) *(b)*

Figure 12. Plot of (a) ρ vs NRMS^2/2, and (b) ρ vs NRMS, showing lines of constant A (Coléou et al., 2013).

Again, the easiest way to understand the motivation for the anomaly indicator A is to look at Figure 12(a), which makes the relationship linear. First, consider the solid red line, the lower bound that corresponds to two traces with the same variance. Table 3 shows the computation of A on this line using equation 10 and shows that A is always equal to zero on this line. The reason that the values are all zero is that we are now looking at the addition of ρ and $NRMS^2/2$ rather than the difference, which gives us a constant of 1/2. By subtracting this constant from the sum, this calibrates the line to zero, which implies that there are no anomalous points on this line.

Rho	NRMS^2/2	(Rho+NRMS^2/2)/2	A
1.0	0.0	0.50	0.0
0.8	0.2	0.50	0.0
0.6	0.4	0.50	0.0
0.4	0.6	0.50	0.0
0.2	0.8	0.50	0.0
0.0	1.0	0.50	0.0
-0.2	1.2	0.50	0.0
-0.4	1.4	0.50	0.0
-0.6	1.6	0.50	0.0
-0.8	1.8	0.50	0.0
-1.0	2.0	0.50	0.0

Table 3. Computation of *A* on the lower bound line.

Now, let's look at the dashed red lines on figure 12(a), which represent lines of constant *A*. By shifting $NRMS^2/2$ by 0.2 we get the dashed red line of constant $A = 0.1$ which starts at $\rho = 1.0$. Table 2 shows the computations that prove that this is correct. Notice that this table stops at $\rho = -0.8$, which corresponds to the end of the dashed red line of with constant *A* equal to 0.1.

Rho	NRMS^2/2 + 0.2	(Rho+NRMS^2/2+0.2)/2	A
1.0	0.2	0.60	0.1
0.8	0.4	0.60	0.1
0.6	0.6	0.60	0.1
0.4	0.8	0.60	0.1
0.2	1.0	0.60	0.1
0.0	1.2	0.60	0.1
-0.2	1.4	0.60	0.1
-0.4	1.6	0.60	0.1
-0.6	1.8	0.60	0.1
-0.8	2.0	0.60	0.1

Table 4. Computation of *A* with $NRMS^2/2$ shifted by 0.2.

Notice that the *A* indicator orthogonal to the *Q* indicator. In the next section, we will apply the theory of both Kragh and Christie (2002) and Coléou et al. (2013) to the Sleipner dataset.

SLEIPNER RESULTS

First, let's look at the method proposed by Kragh and Christie (2002). Figure 13 shows the *NRMS* differences between the base and monitor surveys for the CO_2 injection project at Sleipner. These differences were computed over 1200 msec window between times of 400 and 1600 msec. Note the excellent definition of the expanding CO_2 plume using this repeatability indicator.

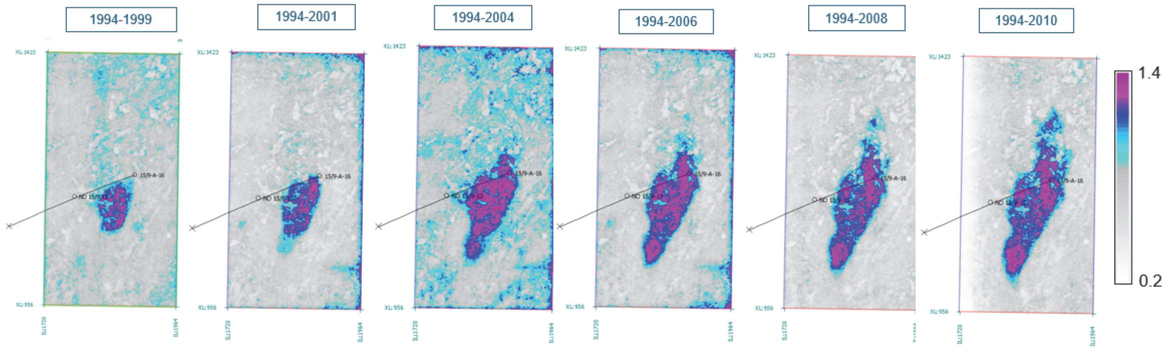

Figure 13. Plot of the NRMS differences between the base and monitor surveys for the CO_2 injection project at Sleipner.

Figure 14 shows the predictability differences between the base and monitor surveys for the CO_2 injection project at Sleipner, again computed over a 1200 msec window between times of 400 and 1600 msec. Again, note the excellent definition of the expanding CO_2 plume using this repeatability indicator. However, if you look at the colour scale you will see it is the reverse of the colour scale shown in Figure 13.

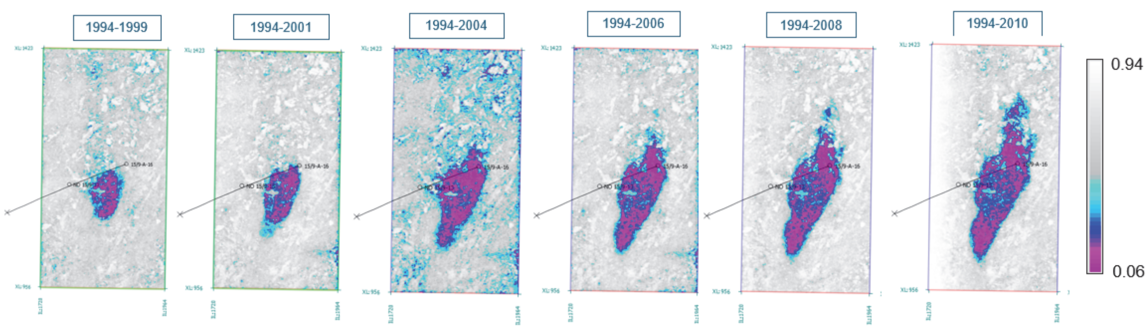

Figure 14. Plot of the predictability differences between the base and monitor surveys for the CO_2 injection project at Sleipner.

Figure 15 shows a cross-plot of *PRED* vs *NRMS* for the 1994 to 2010 survey comparison, where the colour represents crossline number. Notice the excellent agreement between the theory from the previous section (we expect a Gaussian-type shape) and the data display.

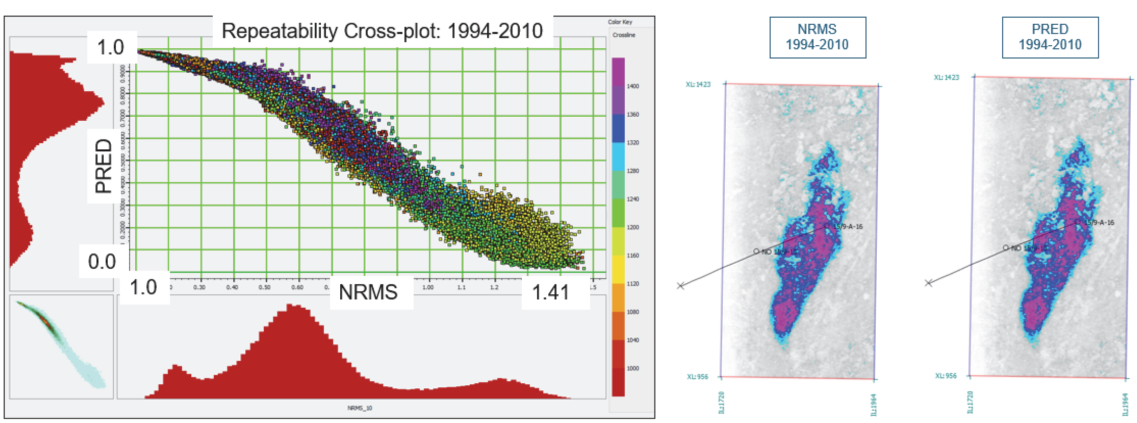

Figure 15. Repeatability cross-plot of PRED vs NRMS for the 1994 to 2010 survey comparison, where the colour represents crossline.

Next, let's pick an elliptical zone on the cross-plot using the anomalous points with low predictability and high *NRMS*, using the central crosslines, as shown in Figure 16. Notice how well the CO_2 plume is defined by this zone.

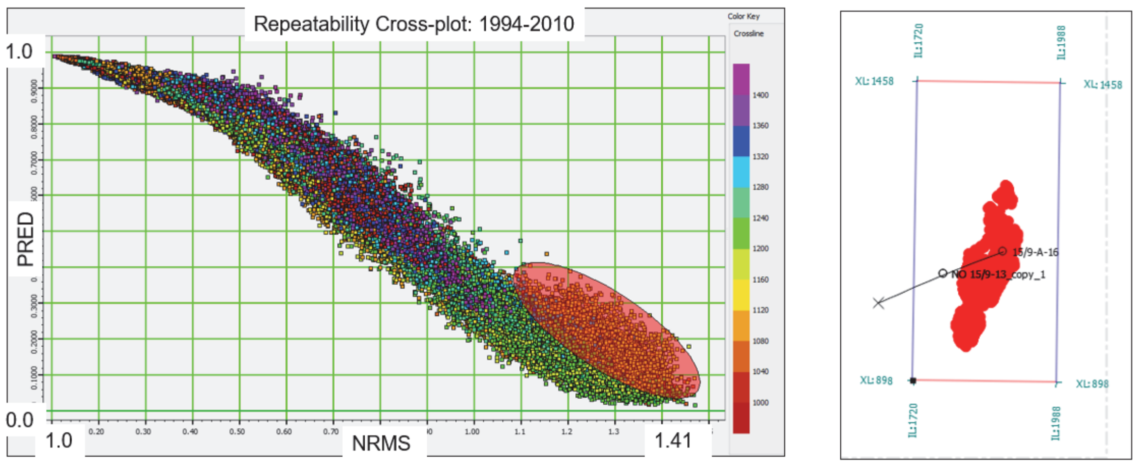

(a) (b)

Figure 16. (a) An elliptical zone around the central crosslines in the plot of Figure 15, where (b) shows the anomalous zone.

Next, let's pick an elliptical zone on the cross-plot using the anomalous points with high predictability and low NRMS, using the upper crosslines, as shown in Figure 17. Now the non-anomalous part of the survey is defined.

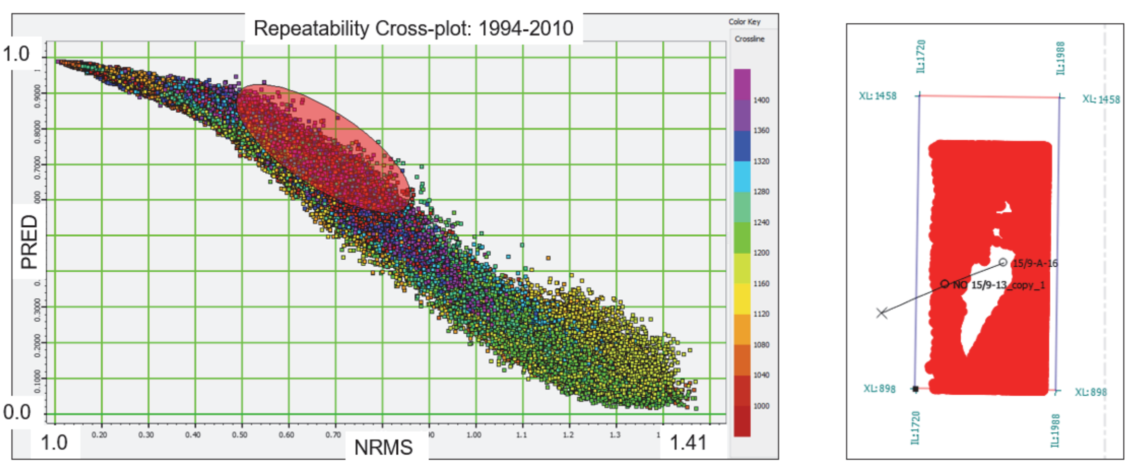

(a) (b)

Figure 17. (a) An elliptical zone picked on the cross-plot using anomalous points with high predictability and low NRMS, using upper crosslines, where (b) shows the resulting anomaly on the map.

Next, let's apply the indicators defined by Coléou et al. (2013). The correlation coefficient between the base and monitor surveys for Sleipner is shown in Figure 18, where the value ranges from 0 (no correlation) to 1 (perfect correlation). These differences were computed over 1200 msec window between times of 400 and 1600 msec, as was done for both the *NRMS* and predictability results shown earlier. The expanding injection plume is clearly defined by low cross-correlation values.

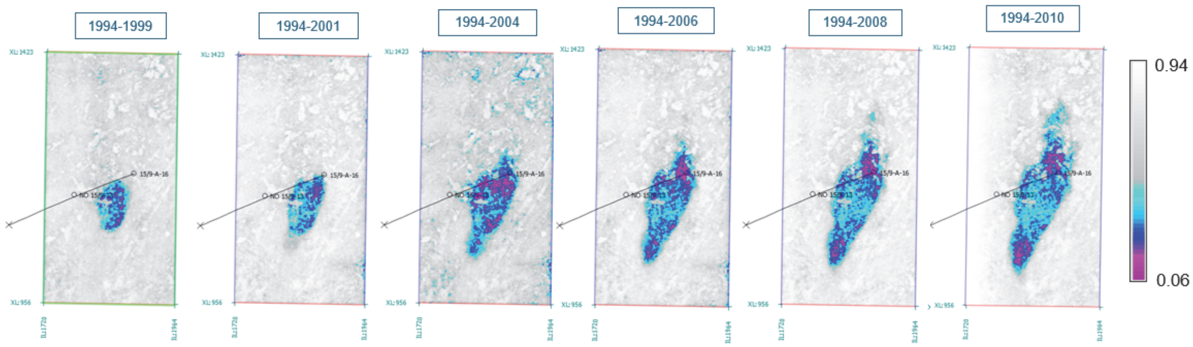

Figure 18. The correlation coefficient between the base and monitor surveys for Sleipner.

Figure 19 shows a cross-plot of ρ versus *NRMS* between 1994 and 2010, with the maps on the left, and the colour scale representing crosslines. Note how well the lower limit of the plot corresponds to the theory.

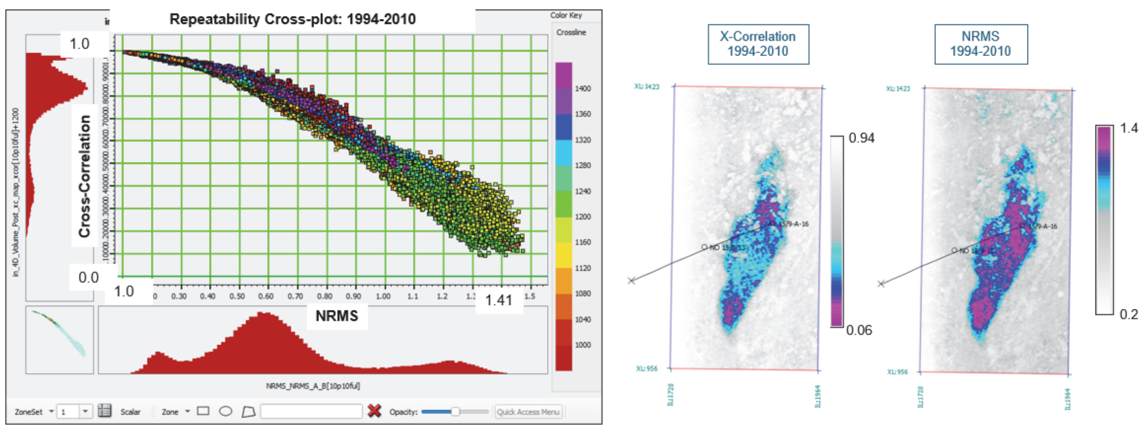

Figure 19. A cross-plot of ρ versus NRMS between 1994 and 2010.

Figure 20(a) shows an elliptical zone picked on the cross-plot from Figure 19 using the middle crosslines. Figure 20(b) shows an anomalous region of the seismic difference, which corresponds very closely to the injection plume.

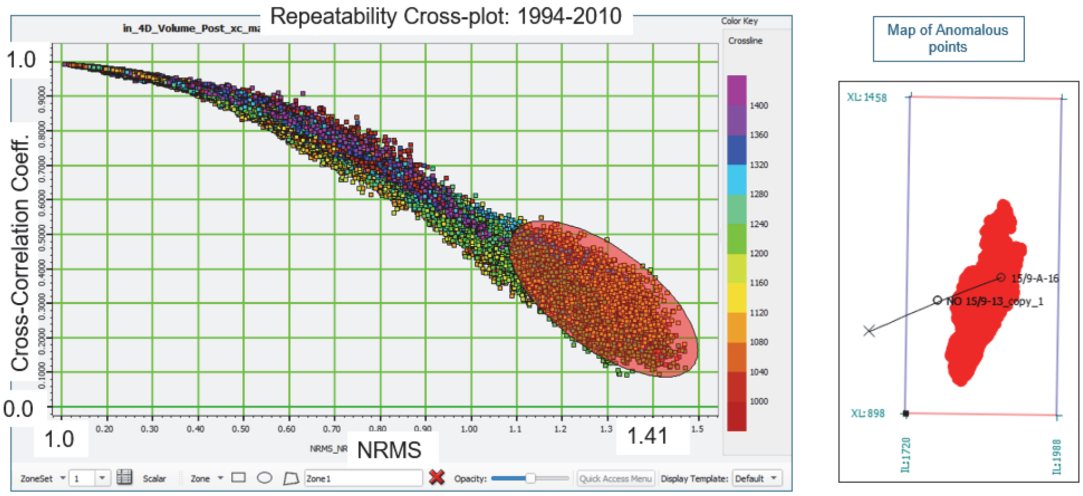

(a) (b)

Figure 20. (a) An elliptical zone around the central crosslines in the plot of Figure 19, where (b) shows the anomalous zone.

Next, we created the quality indicator, Q, and the anomaly indicator A, using the mathematical relationships given in equations 9 and 10. These two maps are shown in Figure 21.

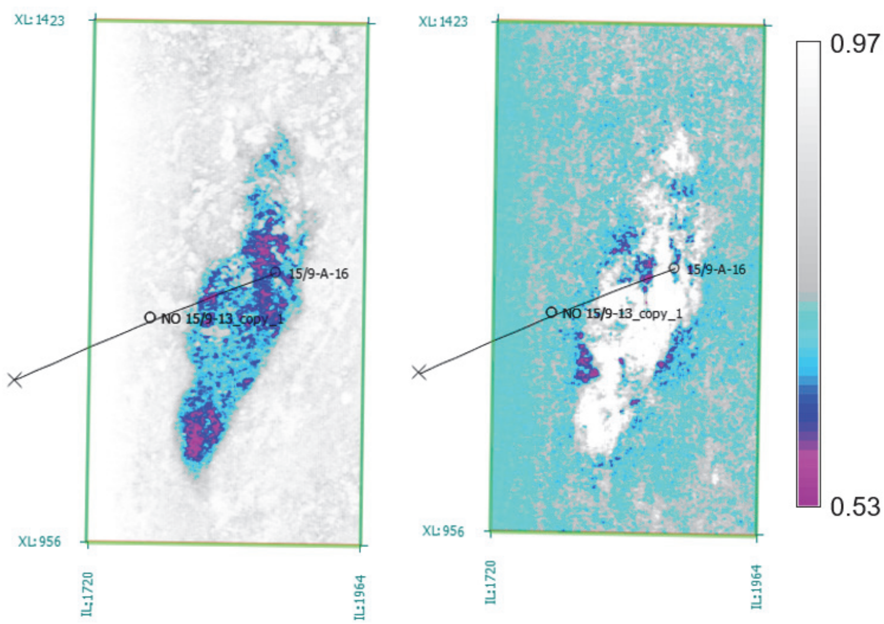

(a) (b)

Figure 21. (a) Quality indicator (Q) map, and (b) anomaly indicator (A) map.

The quality indicator map is very similar to the Cross-Correlation map, but the anomaly indicator shows some interesting features not seen in previous maps.

Next, let's cross-plot these two maps from Figure 21. Figure 22 shows the cross-plot of the two new attributes with Q shown on the vertical axis and A shown on the horizontal axis. The histograms of the two attributes are also shown.

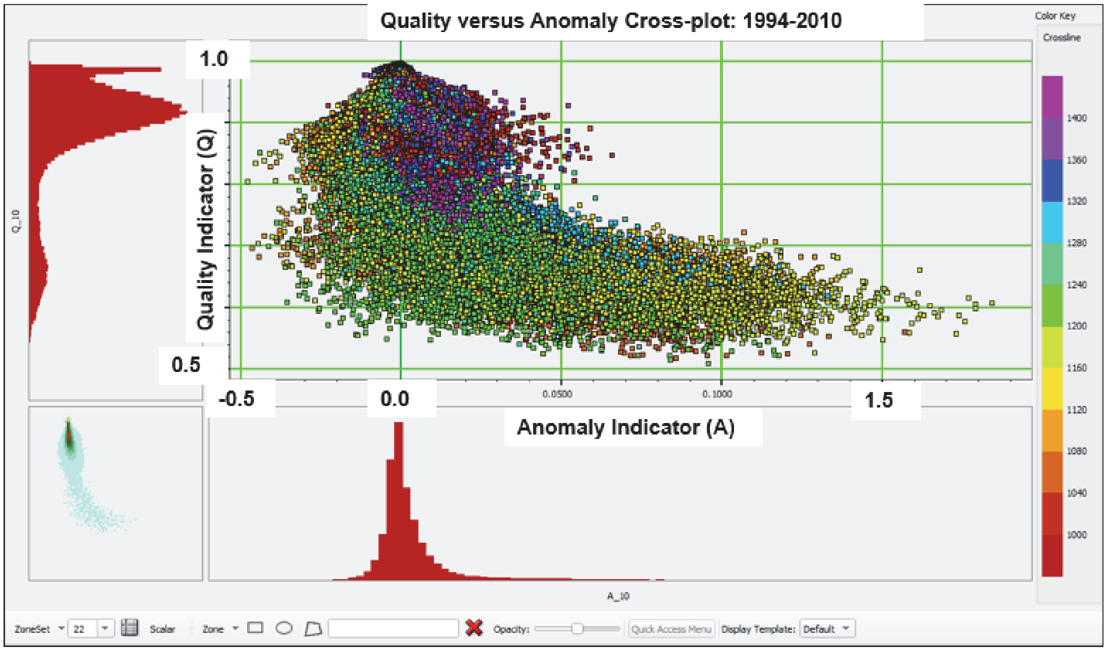

Figure 22. Cross-plot of the Quality attribute Q (on the vertical axis) versus the Anomaly attribute A (on the horizontal axis).

In Figure 23(a), the low values of *Q* from the cross-plot in Figure 22 have been picked, which correspond to the CO_2 plume. The map in Figure 23(b) shows this very clearly.

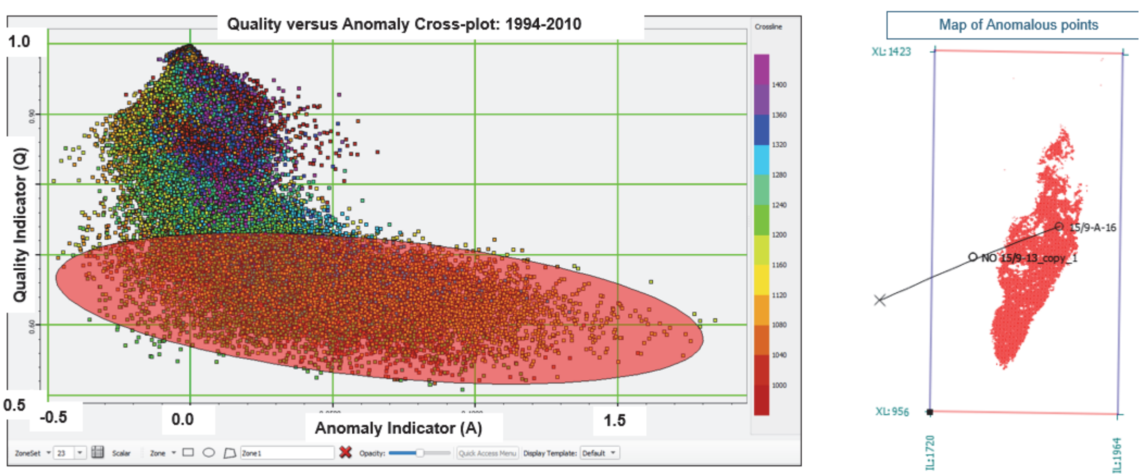

(a) *(b)*

Figure 23. (a) An elliptical zone around the central crosslines in the plot of Figure 21, where (b) shows the anomalous zone.

In Figure 24(a) the high values of *Q* from the map in Figure 22 have been picked, which correspond to the non-anomalous points on the map. This is shown quite clearly in Figure 24(b).

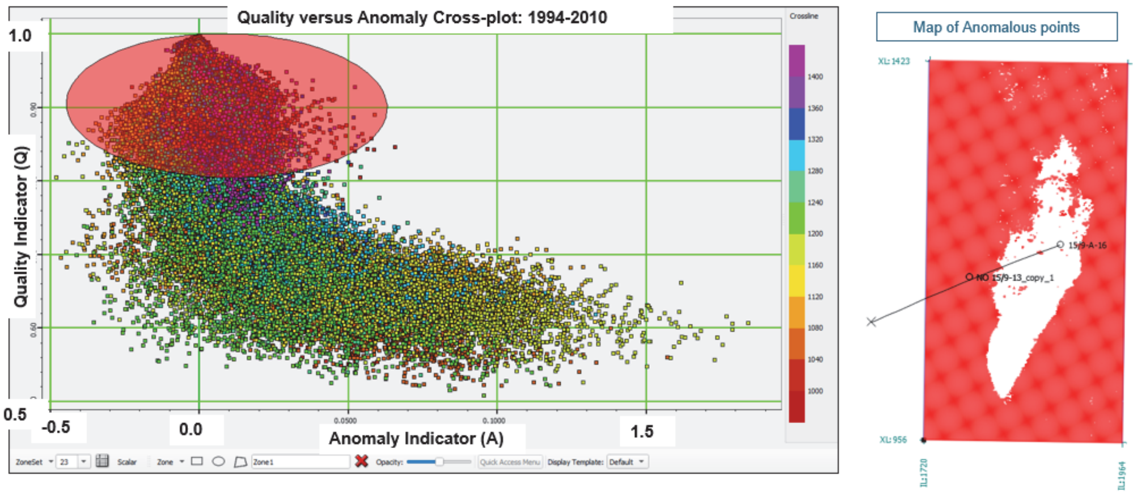

(a) (b)

Figure 24. (a) An elliptical zone around the high crosslines in the plot of Figure 21, where (b) shows the non-anomalous zone.

Finally, Figure 25(a) shows four picked rectangular zones from the cross-plot of Figure 22, where Figure 25(b) shows the corresponding mapped areas. In the map of Figure 25(b), we can now clearly see multiple zones within the anomalous area.

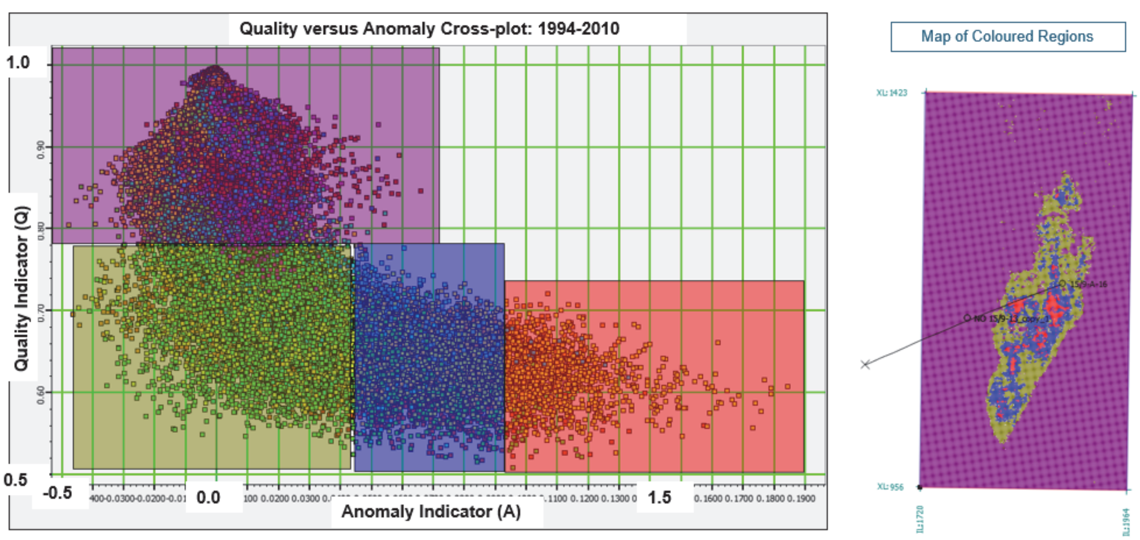

(a) (b)

Figure 25. (a) Four rectangular zones have been picked on the plot of Figure 22, where (b) shows the anomalous zone.

In the map of Figure 25(b), we can now clearly see multiple zones within the anomalous area, where the purple zone defines the non-anomalous area and the green, blue, and red zones define areas of interest within the anomalous area.

DISCUSSION

In this case study I have computed and compared five different repeatability measures using the time lapse data from Sleipner CO_2 storage project in offshore Norway. The well-known repeatability measures were *NRMS*, predictability, and cross-correlation coefficient, or ρ. The lesser-known repeatability measures were quality indicator (Q) and anomaly indicator (A) which, as shown by Coléou et al. (2013), were weighted combinations of *NRMS* and ρ. Figure 26 shows a summary of these 5 repeatability measures, computed over 1200 msec window between the 1994 base survey and the 2010 monitor survey.

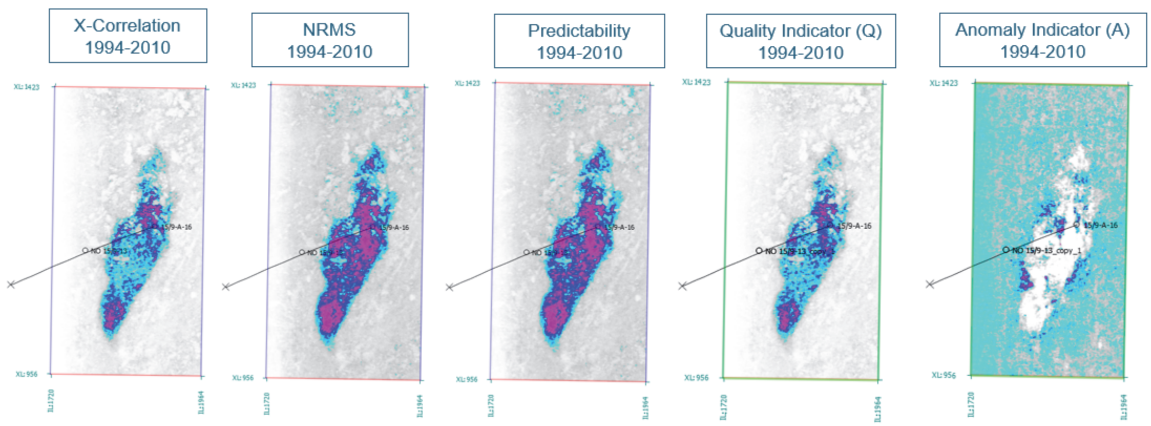

Figure 26. The five major repeatability indicators discussed in this study.

Note the similarity of the cross-correlation coefficient and quality indicator maps, and between the NRMS and predictability maps (although the colour scales are reversed in these two maps, since on NRMS the high values are anomalous and on predictability the low values are anomalous). However, the anomaly indicator map shows interesting features, suggesting it may be a useful new indicator to use.

The real power of these plots is when they are cross-plotted and interrogated using interactive zone picking, as shown in Figure 27.

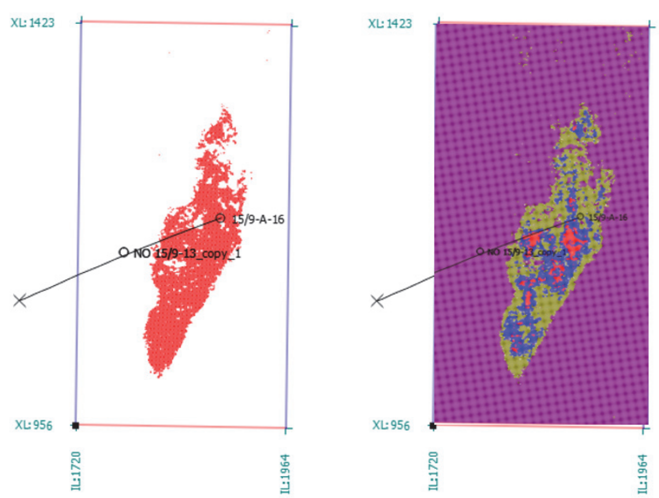

Figure 27. Picking a single zone (left) and multiple zones (right) on a Q vs A cross-plot.

The maps shown in Figure 27 come from Figures 23 and 25 and were created by picking zones on a cross-plot of quality indicator *Q* against anomaly indicator *A*. The map on the left shows the result of picking a single elliptical zone and displays the CO_2 plume quite well. The map on the right shows the result of picking four rectangular zones. The zones in the map on the right in Figure 27 could be matched up with different amount of injected CO_2 within the storage area, and future research will try to identify such zones.

CONCLUSIONS

In this case study, I compared three repeatability measures using the time lapse data from Sleipner CO_2 storage project in offshore Norway: the *NRMS*, predictability, and cross-correlation coefficient techniques. I first reviewed the work of Kragh and Christie (2002) who cross-plotted *NRMS* and predictability and created a random noise model to explain the relationship between the two indicators. Using the Sleipner dataset, I was able show an excellent fit to their theory.

I next reviewed the work of who used a cross-plot of *NRMS* versus cross-correlation coefficient. Coléou et al. (2013) also introduced two new attributes: Quality Indicator (*Q*) and anomaly indicator (*A*). After discussing the relationship between predictability and cross-correlation I then rigorously analyzed the mathematics behind the *Q* and *A* indicators an then applied them to the Sleipner dataset. For each repeatability indicator the anomalous CO_2 plume in Sleipner as a function of time lapse study could be identified, and each indicator gave us a unique perspective on the anomaly.

ACKNOWLEDGEMENTS

The sponsors of CREWES are gratefully thanked for continued support. This work was funded by CREWES industrial sponsors, NSERC (Natural Science and Engineering Research Council of Canada) through the grant CRDPJ 543578-19.

I also thank my colleagues Benjamin Roure, Jon Downton, and Dan Hampson for their input into this presentation.

DEDICATION

Dedicated to the memory of my good friend and former colleague Thierry Coléou, whose original ideas led to the work behind this case study.

REFERENCES

Ghaderi, A., and Landrø, M., 2009, Estimation of thickness and velocity changes of injected carbon dioxide layers from prestack time-lapse seismic data: Geophysics, 74, O17-O28.

Kragh, E., and Christie, P., 2002, Seismic repeatability, normalized rms, and predictability: The Leading Edge, 21, 640 – 647.

Coléou, T., Coulon, J-P, Carotti, D., Dépré, P., Robinson, G, and Hudgens, E, 2013, AVO QC during processing: Presented at the 75th EAGE Conference, London, UK.